

Nodal Line Topological Superfluid and Multiply Protected Majorana Fermi Arc in a Three-Dimensional Time-Reversal-Invariant Superfluid Model

Beibing Huang,^{1,*} Yujie Bai,¹ and Ning Xu^{1,†}

¹*Department of Physics, Yancheng Institute of Technology, Yancheng, 224051, China*

(Dated: November 23, 2021)

We theoretically study a time-reversal-invariant three-dimensional superfluid model by stacking in z direction identical bilayer models with intralayer spin-orbit coupling and contrary Zeeman energy splitting for different layer, which has been suggested recently to realize two-dimensional time-reversal-invariant topological superfluid. We find that this model shows two kinds of topologically nontrivial phases: gapless phases with nodal lines in pairs protected by chiral symmetry and a gapped phase, both of which support time-reversal-invariant Majorana Fermi arc (MFA) on the yz and xz side surface. These MFA abide by time-reversal and particle-hole symmetries and are topologically protected by the winding numbers in mirror subspaces and Z_2 numbers of two-dimensional DIII class topological superfluid, different from MFA in the time-reversal broken Weyl superfluid protected by nonzero Chern number. This important observation means that MFA in our model represents a new type of topological state not explored previously. The Zeeman field configuration in our model is relevant to antiferromagnetic topological insulator MnBi_2Te_4 , thus our work stimulates the further studies on superconducting effects in the realistic antiferromagnetic topological insulator.

INTRODUCTION

Accompanying the hottest discussion on gapped topological phase [1–4], gapless topological phase with Fermi surface has gradually become another studying focus [5, 6]. Considering all ten Altland-Zirnbauer symmetry classes, topologically stable Fermi surfaces with all kinds of codimension p have been classified according to their topological charges from the K-theory [7, 8]. A typical representative explored in various cold atom systems [9–16] and solid state materials [17–29] is three-dimensional (3D) Weyl semimetal/superfluid with codimension $p = 3$, which characterize Weyl point (WP) Fermi surfaces. The WP can be regarded as the magnetic monopole in momentum space [30–32] and topologically protected by nonzero Chern number defined for any two-dimensional (2D) surface enclosing the WP.

The bulk-boundary correspondence signifies the non-trivial surface states in Weyl semimetal/superfluid. For any surfaces not perpendicular to lines connecting WPs, there exists open Fermi arc, which connects projections of the WPs with opposite Chern number on the surface Brillouin zone [17]. In terms of Weyl superfluids, Fermi arc possesses Majorana character and is also denoted by Majorana Fermi arc (MFA) due to inherent particle-hole symmetry (PHS). To our knowledge in all existing models realizing the Weyl superfluid [9–14, 27, 28], time-reversal symmetry (TRS) is explicitly broken, and MFA is protected by nonzero Chern number.

In this work, we suggest a 3D theoretical model to study MFA not protected by nonzero Chern number. Our main results are as followings. The suggested model realizes two kinds of topologically nontrivial phases, both of which support MFA. The first kind of phase is gapless. Different from Weyl superfluids, this gapless phase has nodal lines instead of WPs. The topological sta-

bilities of nodal lines are protected by chiral symmetry [7, 33, 34]. By tuning the parameters of the model, these nodal lines disappear in pairs, driving the system into a fully gapped phase, which shows the MFA in the whole Brillouin zone in the z direction and is different from the conventional gapped topological phases. Moreover MFA in two kinds of phases are topologically protected by the winding numbers in mirror subspaces and Z_2 numbers of 2D DIII class topological superfluid, but not nonzero Chern number. This important observation means that MFA in our model represents a new type of topological state not explored previously.

THEORETICAL MODEL

The model we consider can be regarded as 3D extension of a bilayer model with intralayer spin-orbit coupling and contrary Zeeman energy splitting for different layer, which has been suggested recently to realize 2D time-reversal-invariant topological superfluid [35]. Let H_i and \mathcal{V}_i denote single particle Hamiltonian and pairings for i th bilayer, $H_{i,i+1}$ the coupling between i th and $(i+1)$ th bilayers, the Hamiltonian of 3D system is

$$\begin{aligned}
 H &= \sum_i [H_i + \mathcal{V}_i + H_{i,i+1}], \\
 H_i &= \sum_{\mathbf{k}_\perp \alpha \beta s} \psi_{\mathbf{k}_\perp i \alpha s}^\dagger \{ [\epsilon_{\mathbf{k}_\perp} + \Gamma_\alpha \sigma_z + \lambda_y k_y \sigma_x \\
 &\quad - \lambda_x k_x \sigma_y]_{ss'} \delta_{\alpha\beta} - t(1 - \delta_{\alpha\beta}) \delta_{ss'} \} \psi_{\mathbf{k}_\perp i \beta s'}, \\
 \mathcal{V}_i &= -\Delta \sum_{\mathbf{k}_\perp \alpha} \psi_{\mathbf{k}_\perp i \alpha \uparrow}^\dagger \psi_{-\mathbf{k}_\perp i \alpha \downarrow}^\dagger + h.c., \\
 H_{i,i+1} &= -t \sum_{\mathbf{k}_\perp s} \psi_{\mathbf{k}_\perp i \alpha s}^\dagger \psi_{\mathbf{k}_\perp i+1 \beta s} + h.c.
 \end{aligned} \tag{1}$$

where $\psi_{\mathbf{k}_\perp i \alpha s}^\dagger$ is the creation operator for the fermion particle with momentum \mathbf{k}_\perp , spin $s = \uparrow, \downarrow$ and sublayer index $\alpha = 1, 2$ in a bilayer. $\epsilon_{\mathbf{k}_\perp} = \mathbf{k}_\perp^2/2m - \mu$ is in-plane kinetic energy measured from chemical potential μ . The prime over the summation in $H_{i,i+1}$ means that the sublayer indexes are limited to $\alpha = 2$ and $\beta = 1$, i.e. we only consider the nearest neighborhood tunneling between the bilayers. t is the tunneling between different sublayers. We assume the distance between any two nearest layer to be $a/2$, so the length for unit cell in z direction is a . λ_x and λ_y are anisotropic intralayer spin-orbit coupling. Our main investigations are on the isotropic case $\lambda_x = \lambda_y = \lambda$. We will briefly discuss the effects of the anisotropy. Γ_α are sublayer-dependent effective Zeeman energy splittings $\Gamma_1 = -\Gamma_2 = \Gamma$. Such Zeeman field configuration can be relevant to Van der Waals layered material MnBi_2Te_4 [36–38], in which the intralayer exchange coupling is ferromagnetic, giving 2D ferromagnetism in their septuple layer; while the interlayer exchange coupling is antiferromagnetic, forming 3D A-type antiferromagnetism in their bulk. On the other hand this required Zeeman field may also be realized in ultracold atoms using spin-dependent optical lattice [35, 39]. Under the Nambu basis $\Phi_{\mathbf{k}} = (\psi_{\mathbf{k}}, \psi_{-\mathbf{k}}^\dagger)^T$ with $\psi_{\mathbf{k}} = (\psi_{\mathbf{k}1\uparrow}, \psi_{\mathbf{k}1\downarrow}, \psi_{\mathbf{k}2\uparrow}, \psi_{\mathbf{k}2\downarrow})$ and $\mathbf{k} = (\mathbf{k}_\perp, k_z)$, the Hamiltonian H can be arranged into the following Bogoliubov-de Gennes (BdG) equation $H = \frac{1}{2} \sum_{\mathbf{k}} \Phi_{\mathbf{k}}^\dagger H(\mathbf{k}) \Phi_{\mathbf{k}}$ with

$$H(\mathbf{k}) = \begin{pmatrix} \mathcal{H}_0(\mathbf{k}) & \hat{\Delta} \\ \hat{\Delta}^\dagger & -\mathcal{H}_0^*(-\mathbf{k}) \end{pmatrix}, \quad (2)$$

where $\mathcal{H}_0(\mathbf{k}) = \epsilon_{\mathbf{k}_\perp} s_0 \otimes \sigma_0 + \Gamma s_z \otimes \sigma_z - 2t \cos(k_z a/2) s_x \otimes \sigma_x + \lambda_y k_y s_0 \otimes \sigma_x - \lambda_x k_x s_0 \otimes \sigma_y$, $\hat{\Delta} = -i\Delta s_0 \otimes \sigma_y$. $s_{0,x,y,z}$, $\sigma_{0,x,y,z}$ are two sets of Pauli matrices acting on the layer and spin spaces. We will also introduce $\tau_{0,x,y,z}$ as Pauli matrix acting on the particle-hole space. A feature of this Hamiltonian is that it is free in xy plane and constrained by a lattice in z direction.

The Hamiltonian (2) has PHS $\Sigma H^*(\mathbf{k}) \Sigma^{-1} = -H(-\mathbf{k})$ with $\Sigma = \tau_x \otimes s_0 \otimes \sigma_0$ and TRS $\mathcal{T} H^*(\mathbf{k}) \mathcal{T}^{-1} = H(-\mathbf{k})$ with $\mathcal{T} = i\tau_0 \otimes s_x \otimes \sigma_y$. Thus our model belongs to 3D DIII class. The combination of TRS and PHS gives rise to a chiral symmetry $C = i\mathcal{T}\Sigma$ with $CH(\mathbf{k})C^{-1} = -H(\mathbf{k})$. In addition, the model (2) also has spatial inversion symmetry $IH(\mathbf{k})I^{-1} = H(-\mathbf{k})$ with $I = \tau_z \otimes s_0 \otimes \sigma_z$ and mirror symmetries $\mathcal{M}_x H(k_x, k_y, k_z) \mathcal{M}_x^{-1} = H(-k_x, k_y, k_z)$, $\mathcal{M}_y H(k_x, k_y, k_z) \mathcal{M}_y^{-1} = H(k_x, -k_y, k_z)$, $\mathcal{M}_z H(k_x, k_y, k_z) \mathcal{M}_z^{-1} = H(k_x, k_y, -k_z)$ with $\mathcal{M}_x = I\mathcal{T}$, $\mathcal{M}_y = -i\mathcal{T}$ and $\mathcal{M}_z = \tau_0 \otimes s_0 \otimes \sigma_0$. These mirror symmetries are very vital to topological stabilities of MFA in the model (2), as demonstrated below.

POSSIBLE PHASES AND BULK TOPOLOGY

The structure of phase diagram can be obtained from analyzing the determinant of $H(\mathbf{k})$, which can be calcu-

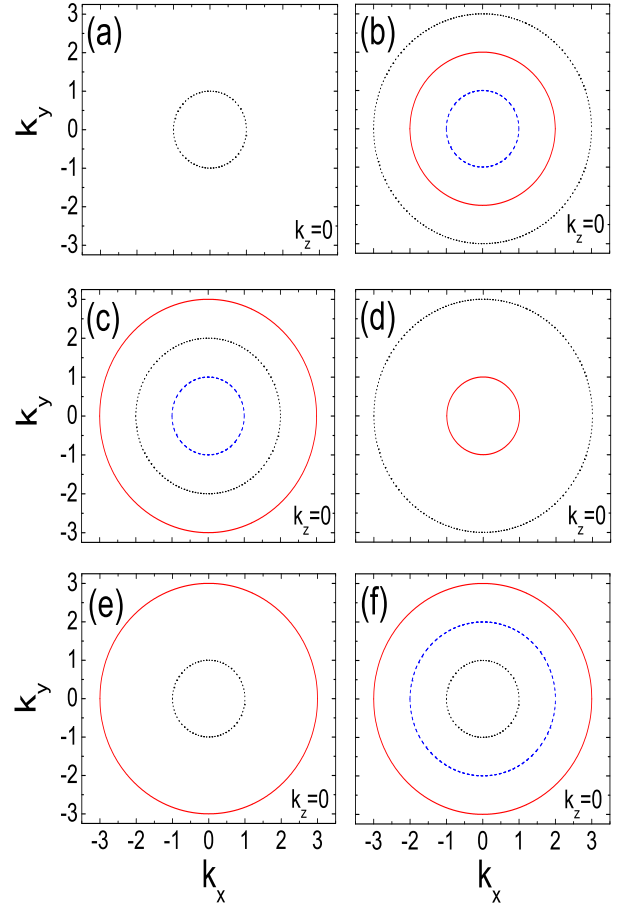


FIG. 1. Possible phases in the model (2). The schematic plots for two equations in (4) at $k_z = 0$ plane. The radius of black circle (dotted) is $2t/\lambda$, while the radii of red (solid) and blue (dashed) circles are $\sqrt{W_c^+}$, $\sqrt{W_c^-}$ if they can be defined. In 3D the red (blue) circle corresponds to an open cylindrical surface along the k_z axis, while the black circle gradually decreases to zero when k_z reaches the boundary of Brillouin zone to form an irregular spherical surface. Thus as long as one of blue and red circles is into the black one, the cylindrical surface(s) will cross irregular spherical surface to form gapless nodal lines of the model (2). From this criterion (a), (e), (f) are gapped phases, (b) is gapless phase with four nodal lines and (c), (d) are gapless phases with two nodal lines. In the maintext, (a) [(e) and (f)] is (are) denoted by gapped phase I (III), while (c) and (d) [(b)] are (is) denoted by gapless phase II (IV).

lated with the help of the chiral symmetry. By finding a unitary matrix $U = (\tau_x \otimes s_x \otimes \sigma_y + \tau_z \otimes s_0 \otimes \sigma_0)/\sqrt{2}$ to diagonalize C that $UCU^\dagger = \tau_z \otimes s_0 \otimes \sigma_0$, we can transform the Hamiltonian into an off-diagonal form

$$UH(\mathbf{k})U^\dagger = \begin{pmatrix} 0 & Q \\ Q^\dagger & 0 \end{pmatrix}, \quad (3)$$

with $Q = \mathcal{H}_0(\mathbf{k}) \cdot (s_x \otimes \sigma_y) - \hat{\Delta}$. Thus $\text{Det}(H(\mathbf{k})) = \text{Det}(Q) \cdot \text{Det}(Q^\dagger) \geq 0$ and the gap closing condition is $\text{Det}(Q) = 0$. Following this method, we find for our

model gap closing signifies that the equations

$$\epsilon_{\mathbf{k}_\perp}^2 + \Delta^2 = \Gamma^2, \lambda^2 \mathbf{k}_\perp^2 = 4t^2 \cos^2 \frac{k_z a}{2} \quad (4)$$

have solutions for \mathbf{k}_\perp and k_z . With the second equation in (4) defining an irregular spherical surface, the first equation defines possible cylindrical surfaces depending on the values $W_c^\pm = 2m(\mu \pm \sqrt{\Gamma^2 - \Delta^2})$. Thus the solutions of (4) correspond to the intersections of spherical surface and cylindrical surfaces and define some gapless nodal lines. Since the number of cylindrical surfaces is at most equal to 2, the maximal number of nodal lines is 4. The relation between all possible phases and parameters $2t/\lambda$, W_c^\pm can be found in Fig.1. Here we notice that the sign of μ affects the phases available. For $\mu < 0$ the maximal number of phases is 3, but for $\mu > 0$ the maximal number of phases is 4.

Below we discuss the topological properties of all phases from the 3D bulk viewpoint. For the gapless phases, there are pairwise nodal lines. The featured structures of nodal lines can be visualized from the circles at $k_z = 0$ plane in Fig.1. To characterize their stabilities, we calculate the winding number [7, 33, 34] $N_1 = \frac{1}{2\pi} \oint_{S^1} d\mathbf{k} \cdot \partial_{\mathbf{k}} \text{Im}[\ln \text{Det}(Q)]$, where the contour S^1 encircles the one of nodal lines from its transverse direction. A nonzero N_1 signifies topological stability. In our model $N_1 = \pm 1$. The topological superfluid with nodal lines can be regarded as the superfluid counterpart of nodal line semimetal widely studied in the solid state materials Ca_3P_2 [40], SrIrO_3 [41], PbTaSe_2 [42] and stable 3D carbon allotrope [43, 44]. While for gapped phase, we could consider a strong topological invariant [3] $N_2 = \int \frac{d^3\mathbf{k}}{24\pi^2} \epsilon^{ijk} \text{Tr}[(Q^{-1} \partial_i Q)(Q^{-1} \partial_j Q)(Q^{-1} \partial_k Q)]$ with $i, j, k = k_x, k_y, k_z$ defined in the whole momentum space, but $N_2 = 0$ due to trivial mirror symmetry \mathcal{M}_z in our model, which leads to $Q(-k_z) = Q(k_z)$ [45]. $N_2 = 0$ means our model cannot realize a strong 3D DIII class topological superfluid, but as illustrated in the next section, the gapped phase III owns anomalous surface states in xz and yz side surfaces, thus it remains topological.

MAJORANA FERMI ARC AND TOPOLOGICAL PROTECTION

In this section surface states on the yz side surface are discussed. We consider a slab with periodic boundary condition in y, z directions and a finite thickness L along x direction. Expanding the wavefunction $\psi(x) = \sum_{n=1}^{\infty} c_n \sin(n\pi x/L)$ [46, 47], the calculated results for $k_y = 0$ are presented in Fig.2. There exists MFA with four fold degeneracy in two gapless phases and gapped phase III.

To correctly illustrate the observed MFA, we introduce two different topological invariants. Firstly we regard 3D system as a set of 2D subsystems, parameter-

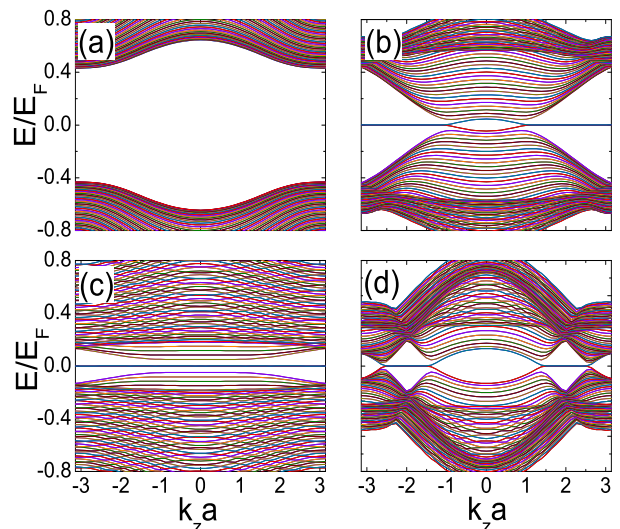


FIG. 2. Surface states on yz side surfaces at $k_y = 0$ for four phases in our model (2). (a)-(d) correspond to phase I-IV, respectively. In (a) $\Gamma = 0.8E_F$, $\Delta = 1.23E_F$, $\mu = -0.07E_F$, (b) $\Gamma = 1.3E_F$, $\Delta = 0.63E_F$, $\mu = -0.11E_F$, (c) $\Gamma = 1.8E_F$, $\Delta = 0.22E_F$, $\mu = -0.43E_F$, (d) $\Gamma = 0.41E_F$, $\Delta = 0.23E_F$, $\mu = 0.42E_F$, with $t = 0.55E_F$, $\lambda k_F = 1.0E_F$. For E_F and k_F , see Fig.3.

ized by the momentum component k_z . Generally the symmetries satisfied by a 3D system must not remain symmetries of 2D subsystem, especially for TRS and PHS, since they correlate the momentum \mathbf{k} with $-\mathbf{k}$ non-locally. However in our model due to trivial MS \mathcal{M}_z [48], TRS $\mathcal{T}H(\mathbf{k}_\perp, k_z)\mathcal{T}^{-1} = H(-\mathbf{k}_\perp, k_z)$ and PHS $\Sigma H(\mathbf{k}_\perp, k_z)\Sigma^{-1} = -H(-\mathbf{k}_\perp, k_z)$ always exist for 2D subsystems. Thus every k_z fixed plane belongs to 2D DIII class and its topological properties can be distinguished by the Z_2 number [49]

$$\nu_2(k_z) = \prod_j [\text{sgn}(\delta_j)]^{p_j}, \quad (5)$$

where p_j is the number of time-reversal-invariant points enclosed by the j -th Fermi surface, $\delta_{j,\mathbf{k}} = \langle j\mathbf{k} | (is_x \otimes \sigma_y) \cdot \hat{\Delta}^\dagger | j\mathbf{k} \rangle$ and $\text{sgn}(\delta_j)$ is the sign of pairing gap on the Fermi surface with $|j\mathbf{k}\rangle$ being the eigenstates of $\mathcal{H}_0(\mathbf{k})$.

Additionally we consider the mirror symmetry \mathcal{M}_y . For $k_y = 0$, the Hamiltonian commutes with \mathcal{M}_y and can be partitioned into two independent mirror subspaces $M_\pm(k_x, k_z) = -\epsilon_{k_x} \sigma_z \otimes \sigma_0 - \Gamma \sigma_z \otimes \sigma_z - (\lambda k_x \pm 2t \cos \frac{k_z a}{2}) \sigma_z \otimes \sigma_y + \Delta \sigma_y \otimes \sigma_y$ under the basis of diagonalizing \mathcal{M}_y [50–54]. Since \mathcal{M}_y anticommutes with TRS and PHS, every mirror subspace belongs to AIII class with the common chiral operator $S = \sigma_x \otimes \sigma_0$. Thus every mirror subspace can be further written into the nondiagonal form

$$M_\pm(k_x, k_z) \sim \begin{pmatrix} 0 & Q_\pm \\ Q_\pm^\dagger & 0 \end{pmatrix} \quad (6)$$

with $Q_{\pm} = \epsilon_{k_x} \sigma_0 - \Gamma \sigma_z - (i\Delta + \lambda k_x \pm 2t \cos \frac{k_z a}{2}) \sigma_y$. In the mirror subspaces, every 1D subsystem can be classified by the winding number

$$N_{\pm}(k_z) = \frac{1}{2\pi} \int_{-\infty}^{\infty} dk_x \partial_{k_x} \text{Im}[\ln \text{Det} Q_{\pm}]. \quad (7)$$

Since two mirror subspaces are correlated with each other by TRS and PHS, the winding numbers $N_{\pm}(k_z)$ are not independent and we can prove exactly $N_+(k_z) = N_-(k_z)$.

We have numerically calculated $\nu_2(k_z)$, $N_{\pm}(k_z)$ and find that two topological invariants are nonzero as long as $\Gamma^2 > [2t^2 \cos^2 \frac{k_z a}{2} / (m\lambda^2) - \mu]^2 + \Delta^2$. In gapped phase I (III), two invariants are trivial (nontrivial) for all k_z fixed subsystems; In gapless phase II, only subsystems with $k_z \in (-\pi/a, -k_z^+) \cup (k_z^+, \pi/a)$ or $k_z \in (-k_z^-, k_z^-)$ are nontrivial, where $\cos(k_z^{\pm} a/2) = \sqrt{\lambda^2 W_c^{\pm} / (4t^2)}$, depending on that the gapless phase II corresponds to Fig.1(b) or Fig.1(d); While in gapless IV only subsystems with $k_z \in (-k_z^-, -k_z^+) \cup (k_z^+, k_z^-)$ are nontrivial. We also find that the range in which two topological invariants are nonzero is exactly the same as that MFA exist, in other words MFA in the model (2) is protected by $\nu_2(k_z)$, $N_{\pm}(k_z)$. No matter which topological invariant protect the MFA in Fig.2, it is different from MFA in the time-reversal broken Weyl superfluid protected by nonzero Chern number. This important observation means that MFA in our model represents a new type of topological state not explored previously. The same MFA also exists in xz surface and can be analyzed similarly if we consider the mirror symmetry \mathcal{M}_x .

PHASE DIAGRAM WITH SELF-CONSISTENT PAIRING GAP

Within BCS mean-field theory, let $-U$ ($U > 0$) denote the effective attraction strength in each layer. Then the pairing gaps $\Delta_{\alpha} = U \sum_{\mathbf{k}} \langle \psi_{-\mathbf{k}\alpha\downarrow} \psi_{\mathbf{k}\alpha\uparrow} \rangle$ and the free energy at zero temperature $F = \frac{1}{2} \sum_{\mathbf{k}} \left[\text{Tr} \mathcal{H}_0(\mathbf{k}) - \sum_{\eta=1}^4 E_{\eta\mathbf{k}} \right] + (|\Delta_1|^2 + |\Delta_2|^2)/U + \mu N$. Here $E_{\eta\mathbf{k}}$ are four positive eigenvalues of BdG Hamiltonian $H(\mathbf{k})$ and N is the particle number. The integral for \mathbf{k}_{\perp} is divergent and we choose to use the relation $1/U = \sum_{\mathbf{k}_{\perp}} (\mathbf{k}_{\perp}^2/m + \varepsilon_b)^{-1}$ with ε_b being the binding energy in 2D free space [55] to regularize F . The physical properties of the ground state can be obtained by minimizing F . Notice that the conclusions of nodal line topological superfluid and multiply protected MFA in model (2) is highly depend on whether the order parameters Δ_{α} of two layers are equivalent. The same magnitudes for Δ_{α} can be directly anticipated from the bilayer's symmetry. In order to check whether Δ_{α} have the same phases, we consider the ansatz $\Delta_1 = \Delta$, $\Delta_2 = \Delta e^{i\phi}$ to investigate the behavior of free energy F as the function of the relative phase ϕ by self-consistently solving order parameter

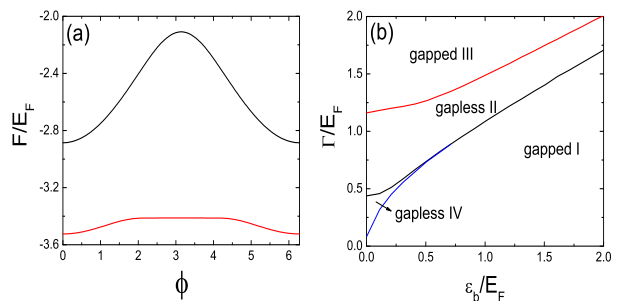


FIG. 3. The landscapes of free energy F as the function of the relative phase ϕ of two order parameters Δ_{α} (a) and phase diagram from the self-consistent calculation (b). In (a) $\varepsilon_b = 1.0E_F$, $\Gamma = 0.8E_F$ for the black (upper) line and $\Gamma = 1.3E_F$ for the red (lower) line. The step structure in the middle of red (lower) line corresponds to the normal state with $\Delta_{\alpha} = 0$. The other parameters are $t = 0.55E_F$, $\lambda k_F = 1.0E_F$. We define the Fermi momentum $k_F = \sqrt{\pi n}$ from particle number density n for every bilayer and Fermi energy $E_F = k_F^2/2m$ as the unit of inverse length and energy. For the definitions of different phases, see Fig.1.

Δ and chemical potential μ . We find that F always obtains minimum at $\phi = 0$. Fig.3(a) shows the landscapes of the free energy for two chosen parameter sets. When $\Delta_1 = \Delta_2$, TRS \mathcal{T} and chiral symmetry C are recovered and our conclusions about bulk topology and MFA are valid. The phase diagram from the self-consistent calculation is shown in Fig.3(b).

DISCUSSIONS

We want to emphasize the following comments. Let us note that the model (2) also have the chiral symmetry C . Thus at $k_y = 0$ we can define similar topological invariant (7) by substituting Q for Q_{\pm} . The numerical results suggest that this winding number is often zero and cannot protect the MFA observed in Fig.2. (This winding number in essence is the same as N_1 , but its integral path cannot embrace the nodal lines.) However this chiral symmetry can protect some other interesting surface states. For example when the projections of nodal lines on certain surfaces do not overlap completely, there are zero-energy Andreev bound states on this surface located within the projected nodal rings [56]. Here we are not interested in them.

In our Hamiltonian, Rashba spin-orbit coupling has been assumed, which ensures flat nodal lines and the same MFA in yz and xz surfaces. However the existences of gapless nodal lines and MFA are also robust for the anisotropic spin-orbit coupling. When we change λ_y (λ_x) slightly, every flat nodal line will develop into a spatial curve and have a finite extension along k_z axis, while the MFA on yz (xz) surfaces will not change when other parameters are fixed. But for a large anisotropy,

the number of nodal lines and MFA can change once the red or blue circle intersects with the black ellipse at $k_z = 0$ in Fig.1. As an example, let us decrease λ_y from Fig.1(e) to induce the crossings. As a result gapped phase III transits into gapless phase II and the MFA in xz surface has the similar structure with Fig.2(b), with the MFA in yz surface invariant. Since a nonzero 2D topological invariant $\nu_2(k_z)$ means the simultaneous presence of edge states in yz and xz surfaces, thus generally for $\lambda_x \neq \lambda_y$ the MFA is only protected by $N_{\pm}(k_z)$. Moreover the above example also demonstrates that for $\lambda_x \neq \lambda_y$ the different phases can own the same MFA in yz or xz surface.

One of the motivations considering sublayer-dependent effective Zeeman energy splittings $\Gamma_1 = -\Gamma_2 = \Gamma$ comes from the recent discovery of layer antiferromagnetic topological insulator MnBi_2Te_4 [36–38]. In the low energy effective model of MnBi_2Te_4 , there are 4 bands for every septuple layer, thus for the antiferromagnetic bilayer there are 8 bands totally; While we only consider a two-band case for the single layer, which is usually used to describe semiconductors or Fermi gases with spin-orbit coupling and is also the starting point for studying D class topological superfluid in 2D [57–59]. Additionally from the 3D perspective the single-particle model of MnBi_2Te_4 has been topological, but it is not true for our model. Although the model (2) is more simple, it has shown lots of exotic quantum phenomena, as demonstrated before. Thus to investigate superconducting effects in the realistic antiferromagnetic topological insulator should be deserved. The superconductivities in time-reversal-invariant topological insulator, Dirac and Weyl semimetal have been widely studied and bring interesting results [60–63].

Experimentally, four kinds of phases in our model can be solely identified by radio-frequency spectroscopy in the cold atom gases and angle-resolved photoemission spectroscopy in condensed matter materials [64–69]. On one hand gapless and gapped phases can be distinguished by nodal lines in the gapless phases, meantime different number of nodal lines can also discriminate different gapless phases. On the other hand in contrast to the gapped phase I, the existence of MFA in gapped phase III enhances the low-energy spectral function and becomes a smoking gun for identifying the different gapped phases.

CONCLUSION

To conclude we theoretically study a time-reversal-invariant three-dimensional superfluid model by stacking a series of bilayers with intralayer spin-orbit coupling and contrary Zeeman energy splitting for different layer. This model shows two kinds of topologically nontrivial phases: gapless phases with nodal lines in pairs protected by chiral symmetry and a gapped time-reversal-invariant

weak topological superfluid phase, both of which support time-reversal-invariant Majorana Fermi arc on the yz and xz side surface, which is topologically protected by the winding numbers in mirror subspaces and Z_2 numbers of two-dimensional DIII class topological superfluid, different from Majorana Fermi arc in the time-reversal broken Weyl superfluid protected by nonzero Chern number. The exotic Majorana Fermi arc predicted here represents a new type of topological state and provides fertile grounds for exploring exotic quantum matters.

Acknowledgements. We would like to thank Ming Gong for discussions. This work is supported by NSFC under Grant No. 11547047 and No. 11704324.

* hbb4236@ycit.edu.cn

† nxu@ycit.cn

- [1] M. Z. Hasan and C. L. Kane, Rev. Mod. Phys. 82, 3045 (2010).
- [2] X.-L. Qi and S.-C. Zhang, Rev. Mod. Phys. 83, 1057 (2011)
- [3] A. P. Schnyder, S. Ryu, A. Furusaki, and A. W. W. Ludwig, Phys. Rev. B 78, 195125 (2008).
- [4] A. Kitaev, AIP Conf. Proc. 1134, 22 (2009).
- [5] P. Hörava, Phys. Rev. Lett. 95, 016405 (2005).
- [6] G. E. Volovik, Universe in a helium droplet (Oxford University Press, 2003).
- [7] Y. X. Zhao and Z. D. Wang, Phys. Rev. Lett. 110, 240404 (2013).
- [8] Y. X. Zhao and Z. D. Wang, Phys. Rev. B 89, 075111 (2014).
- [9] M. Gong, S. Tewari and C. Zhang, Phys. Rev. Lett. 107, 195303 (2011).
- [10] Y. Xu, R.-L. Chu and C. Zhang, Phys. Rev. Lett. 112, 136402 (2014).
- [11] Y. Xu, F. Zhang and C. Zhang, Phys. Rev. Lett. 115, 265304 (2015).
- [12] B. Liu, X. Li, L. Yin and W. V. Liu, Phys. Rev. Lett. 114, 045302 (2015).
- [13] H. Hu, L. Dong, Y. Cao, H. Pu and X.-J. Liu, Phys. Rev. A 90, 033624 (2014).
- [14] X.-J. Liu, H. Hu and H. Pu, Chin. Phys. B 24, 050502 (2015).
- [15] T. Dubček, C. J. Kennedy, L. Lu, W. Ketterle, M. Soljačić and H. Buljan, Phys. Rev. Lett. 114, 225301 (2015).
- [16] J.-H. Jiang, Phys. Rev. A 85, 033640 (2012).
- [17] X. Wan, A. M. Turner, A. Vishwanath and S. Y. Savrasov, Phys. Rev. B 83, 205101 (2011).
- [18] H. Weng, C. Fang, Z. Fang, B. A. Bernevig and X. Dai, Phys. Rev. X 5, 011029 (2015).
- [19] S.-M. Huang et al., Nat. Commun. 6, 7373 (2015).
- [20] S.-Y. Xu et al., Science 349, 613 (2015).
- [21] B. Q. Lv et al., Phys. Rev. X 5, 031013 (2015).
- [22] S.-Y. Xu et al., Nat. Phys. 11, 748 (2015).
- [23] S.-Y. Xu et al., Science Advances 1, e1501092 (2015).
- [24] N. Xu et al., Nat. Commun. 7, 11006 (2016).
- [25] Z. Wang et al., Phys. Rev. B 93, 121112 (2016).
- [26] A. A. Burkov and L. Balents, Phys. Rev. Lett. 107, 127205 (2011).

- [27] T. Meng and L. Balents, Phys. Rev. B 86, 054504 (2012).
- [28] J. D. Sau and S. Tewari, Phys. Rev. B 86, 104509 (2012).
- [29] G. Xu, H. Weng, Z. Wang, X. Dai and Z. Fang, Phys. Rev. Lett. 107, 186806 (2011).
- [30] Z. Fang et al., Science 302, 92 (2003).
- [31] P. Hosur, S. A. Parameswaran and A. Vishwanath, Phys. Rev. Lett. 108, 046602 (2012).
- [32] Y. Chen, D. L. Bergman and A. A. Burkov, Phys. Rev. B 88, 125110 (2013).
- [33] B. Béri, Phys. Rev. B 81, 134515 (2010).
- [34] M. Sato, Y. Tanaka, K. Yada and T. Yokoyama, Phys. Rev. B 83, 224511 (2011).
- [35] B. Huang, P. H. Chui, J. Liu, C. Zhang and M. Gong, arXiv:1511.01713.
- [36] D. Zhang, M. Shi, T. Zhu, D. Xing, H. Zhang and J. Wang, Phys. Rev. Lett. 122, 206401 (2019).
- [37] J. Li, Y. Li, S. Du, Z. Wang, B.-L. Gu, S.-C. Zhang, K. He, W. Duan and Y. Xu, Science Advances 5, eaaw5685(2019).
- [38] M. M. Otrokov, I. I. Klimovskikh, H. Bentmann, et al., arXiv:1809.07389.
- [39] I. H. Deutsch and P. S. Jessen, Phys. Rev. A 57, 1972 (1998).
- [40] L. S. Xie, L. M. Schoop, E. M. Seibel, Q. D. Gibson, W. Xie, and R. J. Cava, APL Mat. 3, 083602 (2015).
- [41] Y. Chen, Y.-M. Lu, H.-Y. Kee, Nat. Commun. 6, 6593 (2015).
- [42] G. Bian, T-R Chang, R. Sankar, et al., arXiv:1505.03069.
- [43] H. Weng, Y. Liang, Q. Xu, R. Yu, Z. Fang, X. Dai, and Y. Kawazoe, Phys. Rev. B 92, 045108 (2015).
- [44] Y. Chen, Y. Xie, S. A. Yang, H. Pan, F. Zhang, M. L. Cohen, and S. Zhang, Nano Lett. 15, 6974 (2015).
- [45] F. Zhang, C. L. Kane and E. J. Mele, Phys. Rev. Lett. 111, 056403 (2013).
- [46] Y. Dong, L. Dong, M. Gong and H. Pu, Nat. Commun. 6, 6103 (2015).
- [47] B. Huang, C. F. Chang and M. Gong, Phys. Rev. B 91, 134512 (2015).
- [48] T. Morimoto and A. Furusaki, Phys. Rev. B 89, 235127 (2014).
- [49] X. Qi, T. L. Hughes and S. Zhang, Phys. Rev. B 81, 134508 (2010).
- [50] C.-K. Chiu, H. Yao and S. Ryu, Phys. Rev. B 88, 075142 (2013).
- [51] H. Yao and S. Ryu, Phys. Rev. B 88, 064507 (2013).
- [52] Y. Ueno, A. Yamakage, Y. Tanaka and M. Sato, Phys. Rev. Lett. 111, 087002 (2013).
- [53] K. Shiozaki and M. Sato, Phys. Rev. B 90, 165114 (2014).
- [54] C.-K. Chiu and A. P. Schnyder, Phys. Rev. B 90, 205136 (2014).
- [55] M. Randeria, J.-M. Duan and L.-Y. Shieh, Phys. Rev. Lett. 62, 981 (1989).
- [56] A. P. Schnyder and S. Ryu, Phys. Rev. B 84, 060504(R) (2011).
- [57] C. Zhang, S. Tewari, R. M. Lutchyn and S. Das Sarma, Phys. Rev. Lett. 101, 160401 (2008).
- [58] M. Sato, Y. Takahashi and S. Fujimoto, Phys. Rev. Lett. 103, 020401 (2009).
- [59] J. D. Sau, R. M. Lutchyn, S. Tewari and S. Das Sarma, Phys. Rev. Lett. 104, 040502 (2010).
- [60] P. Hosur, P. Ghaemi, R. S. K. Mong and A. Vishwanath, Phys. Rev. Lett. 107, 097001 (2011).
- [61] H.-H. Hung, P. Ghaemi, T. L. Hughes and M. J. Gilbert, Phys. Rev. B 87, 035401 (2013).
- [62] S. Qin, L. Hu, X. Wu, X. Dai, C. Fang, F.-C. Zhang and J. Hu, Science Bulletin 64, 1207 (2019).
- [63] Z. Yan, Z. Wu and W. Huang, arXiv:1909.13880.
- [64] Z. Fu, L. Huang, Z. Meng, P. Wang, X.-J. Liu, H. Pu, H. Hu and J. Zhang, Phys. Rev. A 87, 053619 (2013).
- [65] J. Zhang, H. Hu, X.-J. Liu and H. Pu, arXiv:1411.3043 (2014).
- [66] S.-G. Peng, X.-J. Liu, H. Hu and K. Jiang, Phys. Rev. A 86, 063610 (2012).
- [67] Z. Cheng, Z. Zhang, HaigenSun, et al., APL Materials 7, 051105 (2019).
- [68] X.-B. Wang, X.-M. Ma, E. Emmanouilidou, et al., Phys. Rev. B 96, 161112 (2017).
- [69] M. M. Hosen, G. Dhakal, K. Dimitri, et al., Scientific Report 8, 13283 (2018).